1-1-2013

A unique sandwich-structured C/Ge/graphene nanocomposite as an anode material for high power lithium ion batteries

Dan Li
University of Wollongong, danli@uow.edu.au

Kuok H. Seng
University of Wollongong, kseng@uow.edu.au

Dongqi Shi
University of Wollongong, dongqi@uow.edu.au

Zhixin Chen
University of Wollongong, zchen@uow.edu.au

Hua-Kun Liu
University of Wollongong, hua@uow.edu.au

See next page for additional authors

A unique sandwich-structured C/Ge/graphene nanocomposite as an anode material for high power lithium ion batteries

Abstract

A unique sandwich-structured C/Ge/graphene composite with germanium nanoparticles trapped between graphene sheets is prepared by a microwave-assisted solvothermal reaction followed by carbon coating and thermal reduction. The graphene sheets are found to be effective in hindering the growth and aggregation of GeO2 nanoparticles. More importantly, the graphene sheets, coupled with the carbon coating, can buffer the volume changes of germanium in electrochemical lithium reactions. The unique sandwich structure features a highly conductive network of carbon, which can improve both the conductivity and the structural stability of the electrode material, and exemplifies a promising strategy for the development of new high performance electrode materials for lithium ion batteries.

Keywords

power, lithium, ion, batteries, material, high, anode, unique, nanocomposite, graphene, ge, c, structured, sandwich

Disciplines

Engineering | Science and Technology Studies

Publication Details

Li, D., Seng, K. H., Shi, D., Chen, Z., Liu, H. K. and Guo, Z. (2013). A unique sandwich-structured C/Ge/graphene nanocomposite as an anode material for high power lithium ion batteries. Journal of Materials Chemistry A, 1 (45), 14115-14121.

Authors

Dan Li, Kuok H. Seng, Dongqi Shi, Zhixin Chen, Hua-Kun Liu, and Zaiping Guo

Journal of Materials Chemistry A

RSC Publishing

PAPER

View Article Online
View Journal | View Issue

Cite this: J. Mater. Chem. A, 2013, 1, 14115

A unique sandwich-structured C/Ge/graphene nanocomposite as an anode material for high power lithium ion batteries†

Dan Li,[ab] Kuok Hau Seng,[a] Dongqi Shi,[a] Zhixin Chen,[b] Hua Kun Liu[a] and Zaiping Guo*[ab]

Received 21st August 2013
Accepted 25th September 2013

DOI: 10.1039/c3ta13324a

www.rsc.org/MaterialsA

A unique sandwich-structured C/Ge/graphene composite with germanium nanoparticles trapped between graphene sheets is prepared by a microwave-assisted solvothermal reaction followed by carbon coating and thermal reduction. The graphene sheets are found to be effective in hindering the growth and aggregation of GeO_2 nanoparticles. More importantly, the graphene sheets, coupled with the carbon coating, can buffer the volume changes of germanium in electrochemical lithium reactions. The unique sandwich structure features a highly conductive network of carbon, which can improve both the conductivity and the structural stability of the electrode material, and exemplifies a promising strategy for the development of new high performance electrode materials for lithium ion batteries.

Introduction

Recently, the increasing demands on portable and flexible electronic devices have pushed the development of lithium ion batteries with high energy density and power density. Among the electrode materials that have been studied, group IVA materials including silicon, germanium, and tin have attracted extensive attention due to their high theoretical lithium-storage capacities.[1,2] Compared to silicon, germanium has 400 times faster lithium diffusivity[3] and 104 times higher electrical conductivity[4,5] due to its smaller band gap of 0.6 V.[6] It has been proved that the high adsorption energy and low diffusion energy barrier for lithium on the Ge(111) plane could enhance the electrochemical kinetics and decrease the total energy of the system.[7] Therefore, germanium is a promising anode material for lithium ion batteries. Nevertheless, germanium undergoes large volume changes and progressive agglomeration during lithium intercalation/de-intercalation, with a volume expansion of over 300% (ref. 8 and 9) after the full lithiation process (as each Ge atom can accommodate 4.4 Li atoms, leading to the formation of $Li_{22}Ge_5$ alloy). The stresses generated in the process of alloying/de-alloying result in cracking and pulverization of the germanium electrode, and thus a loss of electrical contact and a rapid capacity fade upon cycling.[10]

To circumvent the problem, the strategy of using nanosized structures, nanoparticles,[11] nanowires,[12–15] and nanotubes,[7,16] for example, has been applied to reduce the effects of volume change during charging/discharging in order to improve the cycling stability of the germanium electrodes.[17] In addition, highly porous germanium was fabricated to facilitate lithium ion diffusion at the interfaces between the electrolyte and the active materials, and therefore improves the electrochemical performance.[18] Moreover, germanium alloys such as vertically aligned Si/Ge double-layered nanotube arrays[7] and $Sn_{78}Ge_{22}$@carbon core–shell nanowires[4] showed improved cycling stability due to the reduced maximum hoop strain and lowered activation energy barrier for lithium ion diffusion. The synthesis of these composite materials is always complex and laborious, however, requiring templates and multiple steps.[7]

Carbon coating is a common strategy for the group IVA based anode materials to not only suppress the large volume changes and agglomeration during lithium ion intercalation/de-intercalation, but also improve the electrical conductivity of the electrode.[19–23] In our previous research work, a facile synthesis method was reported for fabricating a series of germanium-based materials, such as Ge/C nanostructures,[24] GeO_2/Ge/C nanocomposites,[25] and hollow ellipsoidal Ge@C nanostructures,[26] *via* carbon coating and reduction of the oxide precursors. More importantly, we found that the particle size of the germanium oxide precursor significantly affects the cycling stability and rate capability. With the nanostructured Ge/C (particles around 30 nm in size),[24] the electrode exhibited an excellent reversible capacity of 480 mA h g^{-1} at a high rate of 40 C, whereas the reference Ge/C (particles about 700 nm in size) showed poor capacity retention when the rate was increased to 5 C and above. Therefore, we believe that very fine

[a]Institute for Superconducting and Electronic Materials, University of Wollongong, Wollongong, NSW 2522, Australia. E-mail: zguo@uow.edu.au; Tel: +61 2 4221 522 5
[b]School of Mechanical, Materials & Mechatronics Engineering, University of Wollongong, NSW 2522, Australia

† Electronic supplementary information (ESI) available. See DOI: 10.1039/c3ta13324a

germanium nanoparticles, uniform carbon coating, and less or no aggregation of these nanoparticles are the key parameters to achieve germanium-based anodes with excellent electrochemical performance.

Furthermore, it has been reported that the agglomeration of particles results in poor electrochemical performance because of the increased diffusion length for lithium ions.[11] Therefore, in this work, graphene has been chosen as a matrix to prevent the growth and aggregation of GeO_2 particles during microwave-assisted solvothermal synthesis. Furthermore, graphene has excellent mechanical properties which can buffer the volume expansion of germanium during lithium ion intercalation/de-intercalation. In addition, graphene provides rapid access to electrons and allows good transportation of lithium ions between the active material and the electrolyte.[27–31] In order to further improve the cycling stability of the composite electrode, a uniform carbon layer is coated on the surface of the germanium–graphene hybrid precursor by thermal decomposition of acetylene gas. Further thermal reduction of the precursors results in the formation of a sandwich structure, where the germanium particles are located between graphene sheets and carbon layers with void space surrounding the germanium particles, which could effectively accommodate the volume expansion of germanium during lithium intercalation. The electrochemical performance of this sandwich structured C/Ge/graphene was evaluated and showed promising results.

Experimental

Graphene oxide (GO) was synthesized from natural graphite powder by a modified Hummers method.[32,33] (The X-ray diffraction (XRD) patterns are shown in Fig. S1 in the ESI.†) 46 mg of the obtained GO was dispersed in 50 mL of anhydrous ethanol by ultrasonication for 0.5 h. 1.072 g (5 mmol) $GeCl_4$ was added to 5 mL anhydrous ethanol and left to stir for 5 minutes. Then, the $GeCl_4$–ethanol solution was added to the as-obtained GO–ethanol solution and left to stir for another 10 minutes. Finally, 30 mL of the resultant mixed solution was transferred into a Teflon-lined autoclave and then irradiated with microwaves at 180 °C for 20 minutes at a fast heating rate of 30 °C min^{-1}. After the solvothermal reaction, a black powder, consisting of GeO_2/graphene, was collected by centrifugation and washed with ethanol and de-ionized water several times before drying it in a vacuum oven at 70 °C overnight. GeO_2 was also synthesized using the same procedure without the addition of GO.

The carbon coating and subsequent reduction processes for the obtained GeO_2/graphene composite were carried out in a tube furnace under flowing acetylene and hydrogen gases, respectively. In a typical experiment, GeO_2/graphene was placed in an alumina crucible in the central part of the heating zone. Vacuum was applied to eliminate air, and the tube was then filled with pure argon gas. The tube furnace was heated to 650 °C at a speed of 5 °C min^{-1}, and a 10% acetylene gas–argon gas mixture was passed through at 200 mL min^{-1}. After 30 minutes of reaction at 650 °C (see XRD patterns of the resultant materials at this stage in Fig. S2†), the acetylene–argon mixture was replaced with 5% hydrogen–argon gas and further reacted for 2 hours to thoroughly reduce the germanium oxide and graphene oxide sheets. Finally, the furnace was left to cool down to room temperature before the samples were removed from the tube furnace. The carbon coating and reduction processes and a

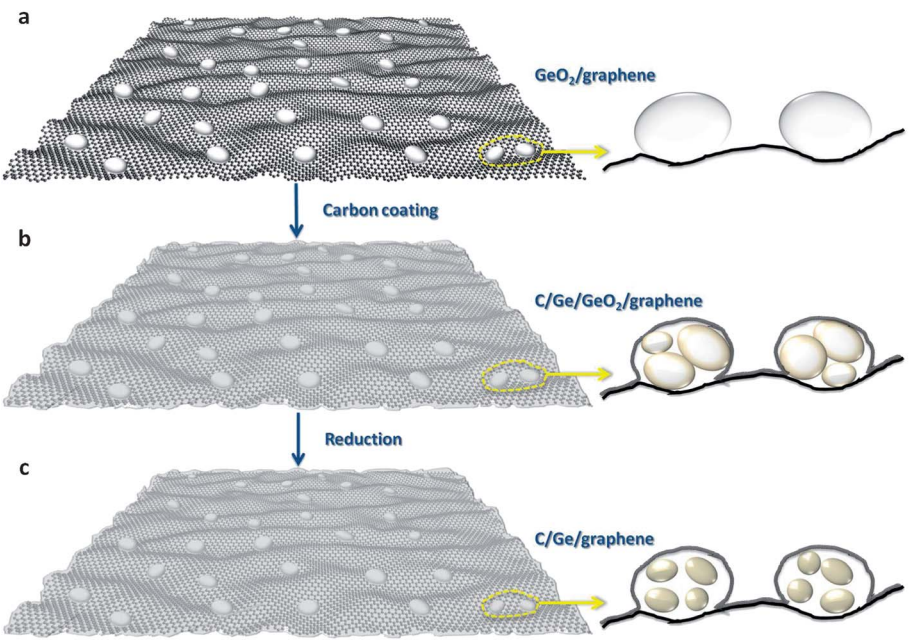

Fig. 1 Schematic illustration of (a) GeO_2/graphene, (b) C/Ge/GeO_2/graphene, and (c) C/Ge/graphene composites. First, the GeO_2/graphene composite was synthesized by a microwave-assisted solvothermal reaction. Then, a uniform carbon layer was coated on the surface of the precursor to form C/Ge/GeO_2/graphene by the decomposition and partial reduction of acetylene gas. After a reduction treatment by hydrogen gas, a unique structured material consisting of metallic germanium nanoparticles between graphene sheets and carbon layers was obtained.

schematic diagram of the sample evolution are presented in Fig. 1. Samples without graphene (Ge/C) and samples without carbon coating (Ge/graphene) were also prepared for comparison.

The crystalline phases of the resulting materials were analyzed by powder X-ray diffraction (XRD, MMA GBC, Australia), which was carried out using Cu Kα radiation (λ = 1.54056 Å) from $2\theta = 10^\circ$ to 80°. Thermogravimetric analysis (TGA) was carried out to determine the carbon content with a TGA/differential scanning calorimetry (DSC) type instrument (METTLER TOLEDO, Switzerland) at a heating rate of 10 °C min^{-1} from room temperature to 800 °C in air. The morphologies and structures of the samples were characterized using a field-emission scanning electron microscope (SEM, JSM-7500FA, JEOL, Japan), and transmission electron microscope (TEM) investigations were performed using a JEOL 2011F analytical electron microscope (JEOL, Japan) operating at 200 keV. X-ray photoelectron spectroscopy (XPS) experiments were carried out on a VG Scientific ESCALAB 2201XL instrument using aluminium Kα X-ray radiation during XPS analysis.

To prepare the working electrode for electrochemical testing, the electrode slurry of C/Ge/graphene was prepared by thoroughly mixing the active material, sodium carboxymethyl cellulose, polyacrylic acid, and acetylene black at a weight ratio of 80 : 5 : 5 : 10 in de-ionized water. For the Ge/C sample, the slurry was made at a weight ratio of 62 : 5 : 5 : 28 in order to keep the same carbon content as in the C/Ge/graphene electrode. The resultant slurry was then spread onto copper foil substrates and dried in a vacuum oven at 150 °C for 3 h. The electrochemical tests were carried out with CR2032 coin type cells. The cells were constructed with lithium foil as the anode, the prepared active material on copper as the cathode, microporous polyethylene (Celgard 2400) as the separator, and 1.15 M $LiPF_6$ in a mixture of ethylene carbonate (EC), dimethyl carbonate (DMC), and diethyl carbonate (DEC) (3 : 4 : 3 by volume) as the electrolyte. The whole assembly process was carried out in an argon-filled glove box (Mbraun, Unilab, Germany). The charge–discharge cycling was performed within the voltage range of 0.01–1.5 V *vs.* Li^+/Li on a battery test instrument (CT2001A, KINGNUO, China) at ambient temperature. Electrochemical impedance spectroscopy (EIS) was conducted by applying a dc potential equal to the open circuit voltage of the cell with an amplitude of 5 mV over the frequency range from 100 kHz to 0.01 Hz. The loading amount of active material for all electrodes was at least 0.9 mg cm^{-2}. The specific capacities were calculated based on the weight of composites, *i.e.* C/Ge, C/Ge/graphene or Ge/graphene.

Results and discussion

The distribution of GeO_2 nanoparticles on the graphene sheets synthesized using the microwave-assisted solvothermal method can be observed from the SEM images of the GeO_2/graphene sample (see Fig. S3(a and b)†). The GeO_2 nanoparticles were found to be anchored on the graphene sheets and uniformly distributed. From TEM analysis of GeO_2/graphene (shown in Fig. S3(c and d)†), the observed GeO_2 nanoparticles are composed of clusters of small particles 20–30 nm in size. Higher magnification images and electron diffraction patterns could not be obtained from the TEM due to the deformation of GeO_2 under focused electron beam irradiation. When GeO_2 was synthesized without the presence of graphene, large hexagonal shaped particles were formed (shown in Fig. S4 and S5†), even though the synthesis conditions were identical. This indicates that graphene provides anchoring sites for GeO_2 and effectively hinders aggregation and further growth of GeO_2 nanoparticles. Fig. 2 shows SEM and TEM images of GeO_2/graphene after carbon coating and thermal reduction treatments (C/Ge/graphene). The SEM image in Fig. 2(a) shows that the morphology of the GeO_2/graphene precursor is maintained. At lower resolution, C/Ge/graphene and GeO_2/graphene look identical, while at higher resolution (shown in Fig. S6(a)†), the germanium particles on the graphene sheets appear to be porous, which is further confirmed by the TEM image of the C/Ge/graphene composite that is shown in Fig. 2(b). As can be seen from Fig. 2(c) and (d), a carbon shell is formed in a shape similar to that in the GeO_2 precursor. The particles inside the shell appeared to have shrunk, however, and voids are observed. This is due to the reduction of GeO_2 to elemental germanium, wherein oxygen is released. In the high-resolution transmission electron microscope (HRTEM) image shown in Fig. S7,† the crystal lattice fringes with a *d*-spacing of 0.33 nm are characteristic of the (111) lattice planes of the cubic germanium, and the germanium nanoparticles are sandwiched between graphene sheets and a thin layer of amorphous carbon (3–5 nm). Furthermore, the morphology of the sample without the carbon coating (Ge/graphene) was also investigated and is shown in Fig. S8.† The germanium particles appear to be attached to the graphene sheets. When compared to C/Ge/graphene, however, the individual particle size of Ge/graphene appears to be larger. This could be due to the role of the carbon coating, which can prevent aggregation of neighboring particles during the reduction process.

The crystal structures of the GeO_2, GeO_2/graphene, Ge/C, Ge/graphene, and C/Ge/graphene samples were characterized

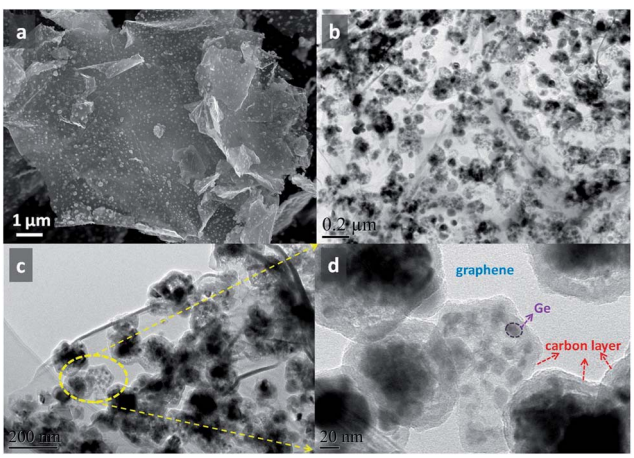

Fig. 2 C/Ge/graphene composite: (a) SEM image; (b–d) TEM images. (d) An enlarged image of the circled area in (c). The purple and red arrows in (d) indicate the germanium nanoparticles and the carbon layer, respectively.

by X-ray diffraction (XRD), as shown in Fig S9† and 3(a). All the reflection peaks of GeO_2/graphene are well indexed to the hexagonal phase of GeO_2 (JCPDS card no. 36-1463). After the reduction treatment, the hexagonal phase is converted to the diamond cubic phase (Ge) (JCPDS card no. 40-0545). There are no peaks corresponding to carbon that can be detected in the pattern, which could be attributed to their overlapping with the (111) peak of germanium at around 27°. The carbon content of the GeO_2/graphene precursor, C/Ge/graphene, and Ge/C composites was investigated by thermogravimetric analysis (TGA), and the calculated values are 19.6 wt%, 10.1 wt%, and 30.3 wt%, respectively, as shown in Fig. S10.† Raman spectroscopy (Fig. 3(b)) was applied to analyze the chemical bonding in the composites due to its high sensitivity to electronic structure.[34] For the GeO_2/graphene precursor, the band at 445 cm^{-1} corresponds to the symmetric Ge–O–Ge stretching.[24] The peak at 302 cm^{-1} is attributed to the optical mode of crystalline germanium, which shows a small blue-shift compared to the reported value of 298 cm^{-1},[11,17,35] indicating the interaction between germanium and the carbon material.[36] Besides, there is a strong D band at 1333 cm^{-1} related to the presence of defects, as well as a G band at 1601 cm^{-1} that is ascribed to the E_{2g} vibrational mode for the sp^2 domain.[37] There is a shift of the G peak which can be observed after carbon coating, from 1598 cm^{-1} for GeO_2/graphene and Ge/graphene to 1601 cm^{-1} for C/Ge/graphene and 1604 cm^{-1} for Ge/C. Combining this with the blue-shift of Ge–Ge stretching, we believe that the charge transfer has occurred between germanium and the carbon components, including both the graphene sheets and the carbon layer,[11,17,35,38] indicating that the germanium nanoparticles are not just physically connected to the graphene sheets and carbon layers, but interact with the carbon network, including both the graphene and the carbon layer, by the formation of bonds.[38]

XPS measurements provide direct information on the element distribution and chemical composition of the surface layer of the obtained composites, as shown in Fig. 3(c). For the GeO_2/graphene precursor, the characteristic peak of Ge 3d at 32.6 eV is assigned to the Ge 3d Ge–O bonds. After reduction treatment, the characteristic peak of zero-valence germanium appears at a binding energy of 29.5 eV. The C 1s XPS spectrum of GeO_2/graphene (Fig. 3(d)) can be deconvoluted into three peaks. The main peak at 284.5 eV can be assigned to sp^2 hybridized C atoms in graphene, while the higher energy peaks arise from C–OH at 286.2 eV and C═O at 288.6 eV.[34,39] These kinds of oxygen-containing groups could provide suitable attachment sites for anchoring Ge^{4+} ions on graphene sheets. After carbon coating, the C–OH and C═O peaks fade away, whereas the C–C bonds become dominant, with a small tail peak in the higher binding energy region. Peaks also appear at 285.5 and 289.8 eV, which can be attributed to sp^3 hybridized C and COOH, respectively. The disappearance of C–OH in the composite might suggest that the formation of C–O–Ge bonds originates from substitution of hydrogen by Ge^{4+}.[38,40] The atomic ratio of germanium to carbon elements can be calculated through the rough stoichiometry according to the XPS

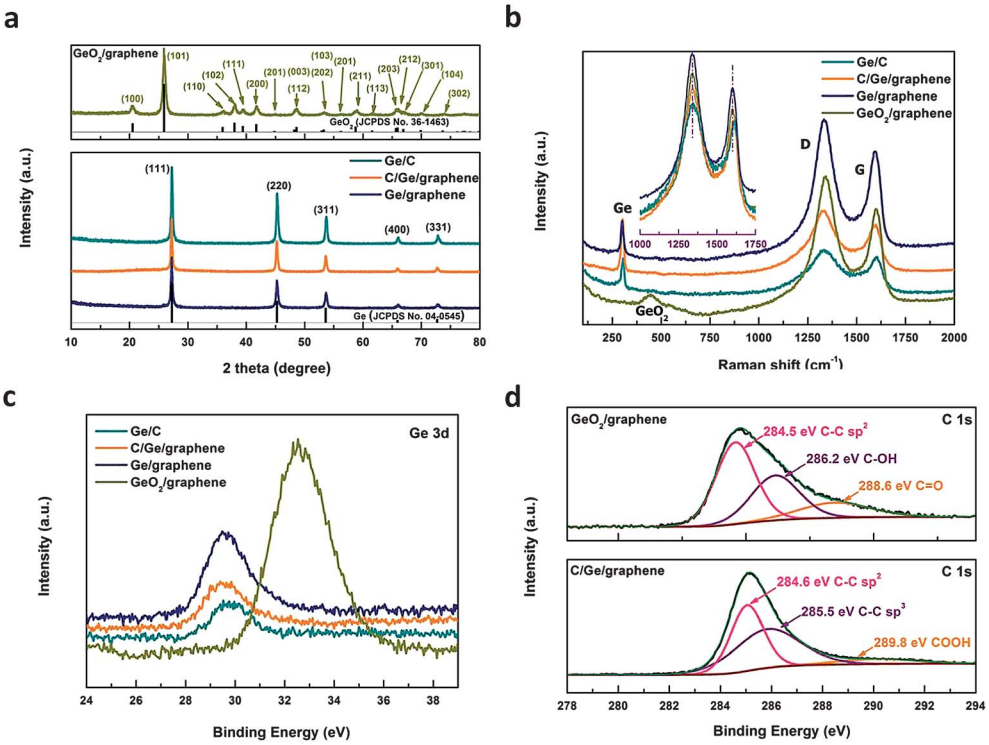

Fig. 3 (a) Powder X-ray diffraction patterns of the samples; (b) Raman spectra, with the inset showing an enlargement of the D and G bands; (c) XPS spectra of Ge 3d element peaks of Ge/C, Ge/graphene, and C/Ge/graphene composites; and (d) curve fittings of C 1s XPS spectra of the GeO_2/graphene precursor and C/Ge/graphene composite.

spectrum, and the ratios for GeO_2/graphene and C/Ge/graphene are 21.81 mol % and 1.63 mol %, respectively. The low germanium to carbon ratio for C/Ge/graphene can be attributed to the uniform carbon coating on the surface of the composite that is created by the thermal carbonization process. Furthermore, the ratio of the oxidized carbon to the non-oxygenated carbon decreases from 31.96% for GeO_2/graphene to 8.10% for C/Ge/graphene, indicating that less oxygen-containing groups exist on the surface of the composite after the carbon coating and reduction processes.

The electrochemical properties of Ge/C, Ge/graphene, and C/Ge/graphene composites as potential anode materials for lithium ion batteries were investigated, and the results are shown in Fig. 4. Fig. 4(a) presents the rate capability of the three composites at different current rates (charging at 0.2–40 C and discharging at 0.4 C). The current density of 1 C rate is 1600 mA g^{-1}. The C/Ge/graphene composite showed the best rate capability. There was a negligible capacity drop when the charging current was increased from 0.2 C to 5 C. The discharge capacity was 1015.3 mA h g^{-1} at the 10^{th} cycle at the rate of 0.2 C, and 1007.6 mA h g^{-1} at the 30^{th} cycle at the rate of 5 C. It is noteworthy that the superior rate capability of the C/Ge/graphene composite is more evident at higher charge–discharge rates. Even at the high rate of 20 C, the specific capacity remains 746.3 mA h g^{-1}, which is still 68% of its capacity at 0.2 C. When the rate was decreased to 0.2 C, the specific capacity recovered

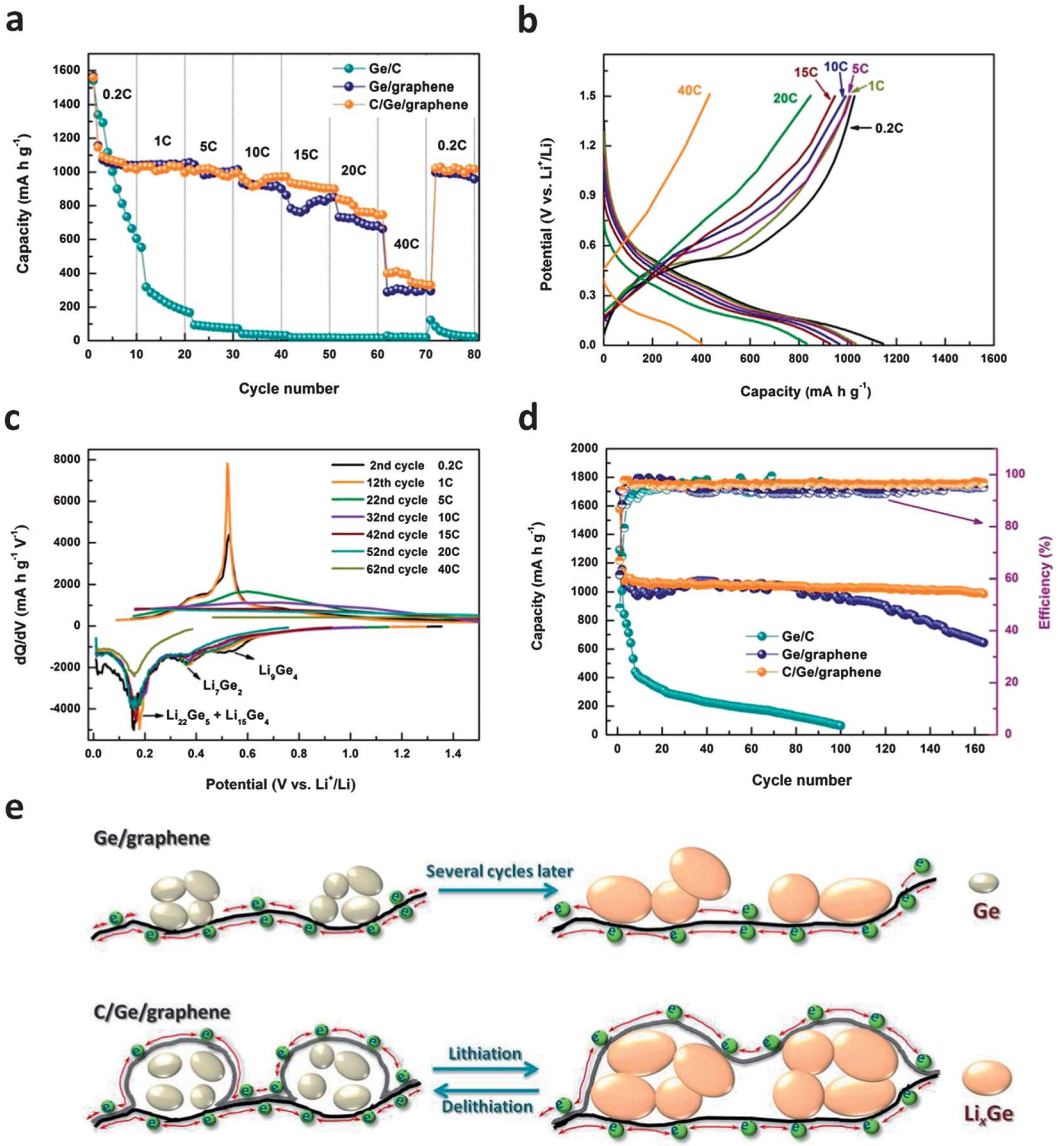

Fig. 4 Comparison of rate capability of Ge/C, Ge/graphene, and C/Ge/graphene composites at different current densities: (a) charging rates from 0.2–40 C, with discharge at 0.4 C, (b) galvanostatic charge–discharge profiles of the C/Ge/graphene composite at different current densities from 0.2–40 C (corresponding to (a)), (c) differential capacity plots of C/Ge/graphene at different cycles. (d) Cycling performance and coulombic efficiency of Ge/C, Ge/graphene, and C/Ge/graphene composites at the charging rate of 1 C and discharging rate of 0.4 C. (e) Schematic illustration of the mechanically robust and flexible matrix composed of the graphene sheets and carbon coating during lithiation/de-lithiation of C/Ge/graphene, compared to the peeling off of Li_xGe formed in the Ge/graphene composite after cycling.

to 1020.6 mA h g^{-1}, indicating good reversibility. The differential capacity plots of the C/Ge/graphene composite at the 2nd and 72nd cycles at the 0.2 C rate are shown in Fig. S12.† The Ge/graphene sample showed poorer capacity retention than the C/Ge/graphene sample when the rate was increased to 10 C and above. As for Ge/C, the electrode presented the worst rate capability compared to C/Ge/graphene. A capacity of 98 mA h g^{-1} was delivered at a current rate of 5 C, with an extremely low retention of 9.7%.

Fig. 4(b) shows the charge–discharge profiles of the C/Ge/graphene composite electrode in the 2nd, 11th, 21st, 31st, 41st, 51st, and 61st cycles at different rates. The corresponding differential plots of C/Ge/graphene at different cycles are shown in Fig. 4(c). From the discharge curve of the second cycle, the lithiation peaks appeared at about 0.55, 0.37, and 0.15 V, corresponding to the formation of Li_9Ge_4, Li_7Ge_2, $Li_{15}Ge_4$, and $Li_{22}Ge_5$.[8,41] The peak at 15 mV is characteristic of graphene lithiation.[42] Fig. 4(d) shows the cycling performance and the coulombic efficiency of the C/Ge/graphene, Ge/graphene, and Ge/C composites. The C/Ge/graphene composite exhibits a discharge capacity of 1578 mA h g^{-1} at the first cycle for a charging rate of 1 C and a discharging rate of 0.4 C, which is close to the theoretical capacity of germanium. The high initial capacity is attributed to the large electrochemically active surface area of graphene and the carbon layer, and/or the grain boundary area of germanium nanoparticles.[29] There is no significant capacity fade from the second discharge cycle. The capacity still remains 992.8 mA h g^{-1} after 160 cycles, corresponding to 86.4% of the capacity at the second cycle. For the sample of Ge/graphene, there was an obvious capacity fading after 90 cycles, and the specific capacity dropped to 643.9 mA h g^{-1} at the 160th cycle, which is 64% of the capacity at the second cycle. The electrochemical performance of our C/Ge/graphene is better than that of the Ge NP/GR nanocomposites reported by Cheng *et al.*,[9] the Ge–RGO hybrids reported by Park *et al.*,[43] as well as the Ge@C/RGO nanocomposite reported by Guo *et al.*[17] The inferior electrochemical performance of Ge/graphene compared to that of C/Ge/graphene can be ascribed to the detachment of germanium or Li_xGe on the graphene sheets after prolonged cycling through the charge–discharge processes. The large volume changes of germanium during alloying/de-alloying contribute not only to the peeling off of nanoparticles from the graphene sheets but also towards pulverization of the electrode (as shown in Fig. 4(e)). The capacity of Ge/C dropped dramatically with increasing cycle number, with a value of 44.5 mA h g^{-1} at the 100th cycle. The poor cycling stability is due to the germanium particles, which tend to aggregate, and the inherently insufficient carbon layer cannot maintain integrity during alloying/dealloying as shown in Fig. S13†, resulting in poor rate capability and cycling performance.

We believe that the excellent electrochemical performance of C/Ge/graphene is attributable to the unique sandwich structure. Firstly, the small size (20–30 nm) and uniform distribution of germanium nanoparticles between the graphene and the carbon layer framework promote fast lithium ion diffusion due to the shortened transport length. Secondly, the electrical conductivity of the composite material is enhanced as a result of the participation of graphene and the additional carbon coating in forming a conductive network. Thirdly, the high structural stability of the composite material owing to the synergistic effects of the graphene sheets and carbon layers which sandwich the germanium nanoparticles protects them from peeling off and further pulverization. This kind of unique structure is specifically beneficial to the increase of electrochemical performance of the group IVA materials, which undergo a large volume change during the alloying/dealloying process, by preventing the direct exposure of the embedded metal nanoparticles to the electrolyte as reported.[44] Moreover, the voids that appear around the germanium nanoparticles after reduction treatment can provide free space for volume expansion.

Conclusions

In summary, a C/Ge/graphene composite was synthesized by a microwave-assisted solvothermal reaction, and then a carbon coating layer was introduced on the surface of the germanium graphene precursor, which was then subjected to a reduction treatment. The as-obtained composite revealed a uniform distribution of very fine germanium nanoparticles 20–30 nm in size between the graphene sheets and the carbon layers. The unique sandwich structure effectively buffers the volume changes during lithium ion intercalation/de-intercalation processes, so that the composite maintains its structural integrity, as well as ensures favorable transport kinetics for both lithium ions and electrons. Therefore, C/Ge/graphene composites exhibit excellent lithium storage performance, with high reversible capacity, excellent rate capability, and superior cycling retention.

Acknowledgements

This work is supported by an Australian Research Council (ARC) Discovery project (DP1094261). Use of facilities within the Electron Microscopy Centre (UOW) is acknowledged. The authors would like to thank Dr Tania Silver for critical reading of the manuscript and valuable remarks.

Notes and references

1 B. Luo, B. Wang, X. Li, Y. Jia, M. Liang and L. Zhi, *Adv. Mater.*, 2012, **24**, 3538.
2 B. Luo, B. Wang, M. Liang, J. Ning, X. Li and L. Zhi, *Adv. Mater.*, 2012, **24**, 1405.
3 J. Graetz, C. C. Ahn, R. Yazami and B. Fultz, *J. Electrochem. Soc.*, 2004, **151**, A698.
4 H. Lee and J. Cho, *Nano Lett.*, 2007, **7**, 2638.
5 M.-H. Park, K. Kim, J. Kim and J. Cho, *Adv. Mater.*, 2010, **22**, 415.
6 D. Wang, Y.-L. Chang, Q. Wang, J. Cao, D. B. Farmer, R. G. Gordon and H. Dai, *J. Am. Chem. Soc.*, 2004, **126**, 11602.
7 T. Song, H. Cheng, H. Choi, J.-H. Lee, H. Han, D. H. Lee, D. S. Yoo, M.-S. Kwon, J.-M. Choi, S. G. Doo, H. Chang,

J. Xiao, Y. Huang, W. I. Park, Y.-C. Chung, H. Kim, J. A. Rogers and U. Paik, *ACS Nano*, 2011, **6**, 303.
8 A. M. Chockla, M. G. Panthani, V. C. Holmberg, C. M. Hessel, D. K. Reid, T. D. Bogart, J. T. Harris, C. B. Mullins and B. A. Korgel, *J. Phys. Chem. C*, 2012, **116**, 11917.
9 J. Cheng and J. Du, *CrystEngComm*, 2012, **14**, 397.
10 R. Teki, M. K. Datta, R. Krishnan, T. C. Parker, T.-M. Lu, P. N. Kumta and N. Koratkar, *Small*, 2009, **5**, 2236.
11 G. Cui, L. Gu, L. Zhi, N. Kaskhedikar, P. A. van Aken, K. Müllen and J. Maier, *Adv. Mater.*, 2008, **20**, 3079.
12 C. K. Chan, X. F. Zhang and Y. Cui, *Nano Lett.*, 2007, **8**, 307.
13 M.-H. Seo, M. Park, K. T. Lee, K. Kim, J. Kim and J. Cho, *Energy Environ. Sci.*, 2011, **4**, 425.
14 F.-W. Yuan, H.-J. Yang and H.-Y. Tuan, *ACS Nano*, 2012, **6**, 9932.
15 X. H. Liu, S. Huang, S. T. Picraux, J. Li, T. Zhu and J. Y. Huang, *Nano Lett.*, 2011, **11**, 3991.
16 M.-H. Park, Y. Cho, K. Kim, J. Kim, M. Liu and J. Cho, *Angew. Chem., Int. Ed.*, 2011, **50**, 9647.
17 D.-J. Xue, S. Xin, Y. Yan, K.-C. Jiang, Y.-X. Yin, Y.-G. Guo and L.-J. Wan, *J. Am. Chem. Soc.*, 2012, **134**, 2512.
18 L. C. Yang, Q. S. Gao, L. Li, Y. Tang and Y. P. Wu, *Electrochem. Commun.*, 2010, **12**, 418.
19 Y.-S. Hu, R. Demir-Cakan, M.-M. Titirici, J.-O. Müller, R. Schlögl, M. Antonietti and J. Maier, *Angew. Chem., Int. Ed.*, 2008, **47**, 1645.
20 S.-H. Ng, J. Wang, D. Wexler, K. Konstantinov, Z.-P. Guo and H.-K. Liu, *Angew. Chem., Int. Ed.*, 2006, **45**, 6896.
21 Z. Wen, Q. Wang, Q. Zhang and J. Li, *Adv. Funct. Mater.*, 2007, **17**, 2772.
22 W.-M. Zhang, J.-S. Hu, Y.-G. Guo, S.-F. Zheng, L.-S. Zhong, W.-G. Song and L.-J. Wan, *Adv. Mater.*, 2008, **20**, 1160.
23 K. T. Lee, Y. S. Jung and S. M. Oh, *J. Am. Chem. Soc.*, 2003, **125**, 5652.
24 K. H. Seng, M.-H. Park, Z. P. Guo, H. K. Liu and J. Cho, *Angew. Chem., Int. Ed.*, 2012, **51**, 5657.
25 K. H. Seng, M.-h. Park, Z. P. Guo, H. K. Liu and J. Cho, *Nano Lett.*, 2013, **13**, 1230.
26 L. Li, K. H. Seng, C. Feng, H. Liu and Z. Guo, *J. Mater. Chem. A*, 2013, **1**, 7666.
27 H. Wang, L.-F. Cui, Y. Yang, H. Sanchez Casalongue, J. T. Robinson, Y. Liang, Y. Cui and H. Dai, *J. Am. Chem. Soc.*, 2010, **132**, 13978.
28 X. Wang, X. Cao, L. Bourgeois, H. Guan, S. Chen, Y. Zhong, D.-M. Tang, H. Li, T. Zhai, L. Li, Y. Bando and D. Golberg, *Adv. Funct. Mater.*, 2012, **22**, 2682.
29 Z.-S. Wu, W. Ren, L. Wen, L. Gao, J. Zhao, Z. Chen, G. Zhou, F. Li and H.-M. Cheng, *ACS Nano*, 2011, **4**, 3187.
30 D. Li, D. Shi, Z. Chen, H. Liu, D. Jia and Z. Guo, *RSC Adv.*, 2013, **3**, 5003.
31 D. Wang, D. Choi, J. Li, Z. Yang, Z. Nie, R. Kou, D. Hu, C. Wang, L. V. Saraf, J. Zhang, I. A. Aksay and J. Liu, *ACS Nano*, 2009, **3**, 907.
32 W. S. Hummers and R. E. Offeman, *J. Am. Chem. Soc.*, 1958, **80**, 1339.
33 D. Li, M. B. Muller, S. Gilje, R. B. Kaner and G. G. Wallace, *Nat. Nanotechnol.*, 2008, **3**, 101.
34 P. Han, Y. Yue, Z. Liu, W. Xu, L. Zhang, H. Xu, S. Dong and G. Cui, *Energy Environ. Sci.*, 2011, **4**, 4710.
35 P. Benzi, E. Bottizzo, C. Demaria, G. Infante, G. Iucci and G. Polzonetti, *J. Appl. Phys.*, 2007, **101**, 124906.
36 N. Li, G. Liu, C. Zhen, F. Li, L. Zhang and H.-M. Cheng, *Adv. Funct. Mater.*, 2011, **21**, 1717.
37 J. Shen, Y. Hu, M. Shi, X. Lu, C. Qin, C. Li and M. Ye, *Chem. Mater.*, 2009, **21**, 3514.
38 G. Zhou, D.-W. Wang, L.-C. Yin, N. Li, F. Li and H.-M. Cheng, *ACS Nano*, 2012, **6**, 3214.
39 A. L. M. Reddy, A. Srivastava, S. R. Gowda, H. Gullapalli, M. Dubey and P. M. Ajayan, *ACS Nano*, 2010, **4**, 6337.
40 S. Pei, J. Zhao, J. Du, W. Ren and H.-M. Cheng, *Carbon*, 2010, **48**, 4466.
41 S. Yoon, C.-M. Park and H.-J. Sohn, *Electrochem. Solid-State Lett.*, 2008, **11**, A42.
42 L. Zhi, Y.-S. Hu, B. E. Hamaoui, X. Wang, I. Lieberwirth, U. Kolb, J. Maier and K. Müllen, *Adv. Mater.*, 2008, **20**, 1727.
43 C. H. Kim, H. S. Im, Y. J. Cho, C. S. Jung, D. M. Jang, Y. Myung, H. S. Kim, S. H. Back, Y. R. Lim, C.-W. Lee, J. Park, M. S. Song and W.-I. Cho, *J. Phys. Chem. C*, 2012, **116**, 26190.
44 B. Wang, X. Li, X. Zhang, B. Luo, M. Jin, M. Liang, S. A. Dayeh, S. T. Picraux and L. Zhi, *ACS Nano*, 2013, **7**, 1437.